

# Indocyanine Green and Curcumin Co-Loaded Nano-Fireball-Like Albumin Nanoparticles Based on Near-Infrared-Induced Hyperthermia for Tumor Ablation

This article was published in the following Dove Press journal:  
*International Journal of Nanomedicine*

Puong Thi Thu Pham<sup>1</sup>  
Xuan Thien Le<sup>1</sup>  
Hanju Kim<sup>1</sup>  
Hwang Kyung Kim<sup>1</sup>  
Eun Seong Lee<sup>2</sup>  
Kyung Taek Oh<sup>3</sup>  
Han-Gon Choi<sup>4</sup>  
Yu Seok Youn<sup>1</sup>

<sup>1</sup>School of Pharmacy, Sungkyunkwan University, Suwon, Gyeonggi-do 16419, Republic of Korea; <sup>2</sup>Division of Biotechnology, The Catholic University of Korea, Bucheon, Gyeonggi-do 14662, Republic of Korea; <sup>3</sup>College of Pharmacy, Chung-Ang University, Seoul 06974, Republic of Korea; <sup>4</sup>College of Pharmacy, Hanyang University, Ansan, Gyeonggi-do 15588, Republic of Korea

**Background:** Indocyanine green (ICG) has received considerable interest as a biocompatible organic photothermal agent, and curcumin (Cur) is considered an attractive natural chemopreventive and chemotherapeutic compound. However, the *in vivo* applicability of ICG and Cur is significantly restricted by their poor ability to target tumors and their extremely low solubility.

**Materials and Methods:** To address these problems, ICG/Cur-loaded albumin nanoparticles (ICG-BSA-Cur-NPs) based on the nab<sup>TM</sup> (nanoparticle albumin-bound) technology were applied to neuroblastomas *in vivo*.

**Results:** The fabricated ICG-BSA-Cur-NPs were found to be spherical, ~150 nm in size and highly dispersible and stable in aqueous solution. Approximately 80% of the incorporated ICG and Cur were gradually released from the NPs over 48 h. All formulations of ICG-BSA-Cur-NPs (5–20 µg/mL) showed efficient hyperthermia profiles (up to 50–60°C within 5 min) in response to 808-nm NIR laser irradiation *in vitro* and *in vivo*. Notably, ICG-BSA-Cur-NPs illuminated with 808-nm laser irradiation (1.5 W/cm<sup>2</sup>) showed excellent cytotoxicity toward N2a cells *in vitro* and undisputable antitumor efficacy in N2a-xenografted mice *in vivo*, compared to other tested sample groups (tumor volumes for PBS, BSA-Cur-NPs, free ICG, and ICG-BSA-Cur-NPs groups were 1408.6 ± 551.9, 1190.6 ± 343.6, 888.6 ± 566.2, and 103.0 ± 111.3 mm<sup>3</sup>, respectively).

**Conclusion:** We demonstrate that these hyperthermal chemotherapeutic ICG-BSA-Cur-NPs have potential as a future brain tumor treatment.

**Keywords:** indocyanine green, curcumin, photothermal therapy, albumin nanoparticles, tumor targeting

## Introduction

Photothermal therapy (PTT) has been viewed as an effective way to suppress solid tumors due to hyperthermia-based cell death.<sup>1</sup> Photothermal agents convert light energy into heat, and gold nanorods and gold nanoclusters are known to be effective photothermal agents due to their localized surface plasmon resonances (LSPR).<sup>2,3</sup> However, the clinical use of gold nanoparticles is restricted due to significant tissue accumulation, poor glomerular filtration, and cetyl trimethylammonium bromide (CTAB)-based toxicity.<sup>4–6</sup> Recently, organic photothermal agents have gained great interest as a substitute for gold nanoparticles because these organic agents are

Correspondence: Yu Seok Youn  
Tel +82-31-290-7785  
Email ysyoun@skku.edu

considered to be safer and more biocompatible.<sup>5</sup> In addition, the combined use of photothermal and chemotherapeutic agents has presented great promise due to their synergistic effect in killing tumor cells.<sup>7–9</sup> Moreover, nanoparticles with both types of agents facilitate tumor targeting and thus decrease unnecessary hyperthermal side effects in normal cells.<sup>10–13</sup>

Indocyanine green (ICG: sodium 4-[2-[(1E,3E,5E,7Z)-7-[1,1-dimethyl-3-(4-sulfonatobutyl)benzo[e]indol-2-ylidene]hepta-1,3,5-trienyl]-1,1-dimethylbenzo[e]indol-3-ium-3-yl]butane-1-sulfonate) is a near-infrared (NIR) dye approved by the US Food and Drug Administration (FDA). It has been used clinically for various biomedical applications, including measurement of cardiac output, monitoring of hepatic function and ophthalmic angiography.<sup>14,15</sup> In addition to bioimaging and diagnostic functions, ICG can be utilized as a multifunctional agent to generate heat or reactive oxygen species (ROS) in response to NIR light for PTT or photodynamic therapy, respectively.<sup>16</sup> However, ICG has many problems as a pharmaceutical, such as concentration-dependent aggregation, poor aqueous stability, rapid renal elimination from the body, and low targetability. These drawbacks critically restrict ICG's clinical application, especially in cancer therapy.<sup>17,18</sup> Recently, ICG-loaded albumin nanoparticles have been developed for multi-modal imaging and photothermal therapy along with improving the ICG properties.<sup>17</sup>

Curcumin (Cur: diferuloylmethane), a natural compound derived from turmeric (*Curcuma longa*), is a potential chemopreventive and chemotherapeutic agent.<sup>19–22</sup> A number of antineoplastic mechanisms of curcumin have been suggested. Cur inhibits nuclear factor-kappa beta,<sup>23</sup> which is involved in the pathogenesis of several malignancies. Cur also suppresses the production of many cytokines, including tumor necrosis factor (TNF)- $\alpha$  and interleukin-1 $\beta$ .<sup>24</sup> In addition, Cur induces brain-expressed X-linked (Bex) pro-apoptosis genes.<sup>22</sup> Nonetheless, the bioavailability and clinical efficacy of Cur is restricted due to its extremely poor aqueous solubility, short circulating half-life and relatively high inhibitory concentration toward cancer cells.<sup>25,26</sup>

Albumin is used as an excellent pharmaceutical carrier due to its advantageous properties, such as biodegradability, biocompatibility, non-immunogenicity, high chemical stability, and solubility.<sup>27,28</sup> Also, acting as a dysopsonin, albumin blocks the adsorption of other plasma proteins and hinders macrophage recognition, which extends the blood circulation time of HSA-coated nanoparticles.<sup>29,30</sup> Based on tumor biology, albumin or albumin nanoparticles

can enhance tumor targetability. Particularly, tumor micro-environments passively facilitate the enhanced permeability and retention (EPR) effect that brings circulating nanoparticles into tumor sites.<sup>31</sup> More importantly, the active transport of albumin-bound NPs into tumor cells via the gp60-mediated transcytosis pathway is considered to be a significant mechanism for tumor targeting due to overexpression of two significant albumin-binding proteins: the gp60 receptor on the tumor endothelium and SPARC (secreted protein, acidic and rich in cysteine) in the tumor interstitium.<sup>32–36</sup> In practice, the nab<sup>TM</sup> (nanoparticle albumin-bound)-based paclitaxel formulation, Abraxane<sup>®</sup> (paclitaxel protein-bound, Celgene Corp.: hereafter termed as ABX) (~130 nm), has exhibited much better antitumor efficacy, based on an augmented maximum tolerated dose.<sup>27,35</sup>

Previously, we developed a variety of nab<sup>TM</sup>-based antitumor formulations for treating many cancers.<sup>20,21,37–39</sup> However, the antitumor efficacies of those formulations relied on only chemotherapeutic effects. Herein, we sought to prepare albumin nanoparticles with antitumor efficacies by dual advantages of hyperthermia and a chemotherapeutic agent. To this end, the albumin-bound nanoparticles were considered to be the best single formulation to address the limitations of both ICG and Cur. Therefore, we designed and prepared the ABX-like albumin nanoparticles containing ICG and Cur (hereafter termed ICG-BSA-Cur-NPs) for ablation treatment of tumors based on hyperthermia. The physicochemical properties of ICG-BSA-Cur-NPs were evaluated using relevant spectroscopic analysis and antitumor efficacy of these NPs were analyzed with neuroblastoma N2a cell-xenografted nu/nu mice, in vitro and in vivo.

## Materials and Methods

### Chemicals

ICG was supplied by Tokyo Chemical Industry co., LTD (TCI, Japan). Bovine serum albumin (BSA; 66.5 kDa and ~99%) and curcumin (Cur) were obtained from Sigma-Aldrich (St. Louis, MO, USA). N2a cells were purchased from the Korean Cell Line Bank (Seoul, Korea). Dulbecco's modified Eagle's medium (DMEM), fetal bovine serum (FBS), and penicillin/streptomycin (P/S) were provided by Corning (Corning, NY, USA). LIVE/DEAD<sup>TM</sup> viability/cytotoxicity kits for mammalian cells were obtained from Thermo Fisher Scientific (Rockford, IL, USA). In situ cell death detection kits were obtained from and Roche Diagnostics (Mannheim, Germany). All

other reagents were purchased from Sigma-Aldrich unless otherwise specified.

## Animals

BALB/c nu/nu mice (male, 6 weeks old) were purchased from Hanlim Experimental Animal Laboratory (Seoul, South Korea). Animals were cared for according to the guidelines issued by the National Institutes of Health (NIH) in accordance with the care and use of laboratory animals (NIH publication 80–23, revised in 1996). Mice were grouped based on their treatment and fed under a 12 h light/dark cycle (lights on at 6 am). This study was approved by the Ethical Committee on Animal Experimentation at Sungkyunkwan University.

## Preparation of BSA-Cur-NPs and ICG-BSA-Cur-NPs

BSA-Cur-NPs and ICG-BSA-Cur-NPs were prepared using nanoparticle albumin-bound (nab<sup>TM</sup>) technology with some adjustments.<sup>39</sup> Briefly, aliquots of 50 mg BSA/1.5 mg ICG or 50 mg BSA were dissolved in 5 mL deionized water (DW). Aliquots (2 mg) of Cur was dissolved in 200  $\mu$ L of a 9:1 solution of chloroform and ethanol. These two solutions were gently mixed and crudely homogenized by using a Wise Tis homogenizer HG-15D (DAIHAN Scientific Co, Seoul, South Korea) at 10,000 rpm and then by passing them through a high-pressure homogenizer (EmulsiFlex-B15 device Avestin, Ottawa, Ontario, Canada) for nine cycles at 20,000 psi. After removal of chloroform by rotary evaporator at 40°C for 15 min under reduced pressure, the resulting NPs were mildly centrifuged at 6000 rpm. The supernatant was collected and purified with Ultra centrifugal filter units (MWCO: 100 kDa, Amicon<sup>®</sup> Ultra, Millipore) to remove the unbound ICG and Cur, and was then lyophilized and stored at –20°C until required.

## Characterization of BSA-Cur-NPs and ICG-BSA-Cur-NPs

The average size and the zeta potential of the BSA-Cur-NPs and ICG-BSA-Cur-NPs (each 1 mg/mL DW) were measured using dynamic light scattering (Zetasizer Nano ZS90, Malvern Instruments, Worcestershire, UK) with a 633 nm He-Ne laser beam and a fixed 90° scattering angle. The surface morphology of the NPs was observed by transmission electron microscopy (TEM) with a model JEM-3010 (JEOL, Tokyo, Japan) and field-emission scanning electron

microscopy (FE-SEM) using a JSM7000F model (JEOL, Tokyo, Japan).

The physical stability of the NPs was evaluated based on the maintenance of particle size over 48 h at room temperature. The BSA-Cur-NPs and ICG-BSA-Cur-NPs with various ICG amounts (5, 10, 20  $\mu$ g) were measured at 1, 6, 12, 18, 24, 30, 36, 42, and 48 h using the DLS method described above.

UV-VIS-NIR spectral scans of the samples either in DW or acetonitrile were also recorded with a Synergy<sup>TM</sup> NEO microplate reader (Bio Tek, Winooski, VT, USA).

## Encapsulation Efficiency and Release of ICG and Cur

The encapsulation efficiency of ICG and Cur in the ICG-BSA-Cur-NPs was evaluated using the following protocol. In brief, 1 mg of the lyophilized ICG-BSA-Cur-NPs was dissolved in 0.1 mL DW. To remove BSA from the NPs, 0.9 mL acetonitrile (ACN) was added to the NP suspension, followed by sonication for 30 min and centrifugation at 14,500 rpm for 20 min. Subsequently, the supernatant was withdrawn for quantification. Absorption spectrophotometry at 808 nm was used to measure ICG concentration, while fluorescence spectrophotometry at excitation and emission wavelengths of 420 and 520 nm, respectively, were applied for Cur quantification, which had carefully been validated by the stability-indicating reversed-phase HPLC assay method of our previous work.<sup>40</sup>

To investigate the release profile of Cur and ICG, 20 mg of ICG-BSA-Cur-NPs or BSA-Cur-NPs was dissolved in 2 mL DW and dialyzed with a semipermeable 10 kDa MWCO membrane (Spectrum Labs, Rancho Dominguez, CA, USA) against 1000 mL of 10 mM PBS (pH 7.4) at 37°C. Every 3 h over 2 days, 0.1 mL of the sample inside the dialysis bag was withdrawn and quantified by the methods mentioned above. Importantly, the release of Cur was carefully performed to maintain the sink condition of Cur, considering its solubility at pH 7.4 and at 37°C in PBS ( $348 \pm 3.2$   $\mu$ g/mL) and its detection limit of approximately 0.05  $\mu$ g/mL on the basis of fluorescence spectrometric quantification.<sup>41</sup>

## In vitro Photothermal Imaging

For in vitro photothermal imaging experiments, 1 mL aliquots of PBS, BSA-Cur-NPs, free ICG (5, 10, 20  $\mu$ g), and ICG-BSA-Cur-NPs (each 5, 10, or 20  $\mu$ g equivalent

ICG) were assessed in 1.5 mL Eppendorf tubes and exposed to laser irradiation (808 nm, 1.5 W/cm<sup>2</sup>) for 10 min. The laser spot size was found to be ~1.2 cm. The temperature changes were recorded and observed by a FLIR E85 photothermal camera (FLIR Systems, Inc., Wilsonville, USA)

## Cytotoxicity of ICG-BSA-Cur-NPs

The toxicity of ICG-BSA-Cur-NPs followed by laser irradiation was evaluated using four separate assays including MTT colorimetric, Trypan blue, Live/Dead, and TUNEL (terminal deoxynucleotidyl transferase (TdT)-mediated dUTP nick end labeling) assays. First, the MTT colorimetric assay was conducted using a slight modification of previous methods.<sup>13,20,39</sup> Briefly, N2a cells were seeded in 96-well plates at a density of  $1 \times 10^4$  cells/well. Following 24 h of incubation, the cells were treated with various concentrations of free ICG, ICG-BSA-Cur-NPs, and BSA-Cur-NPs. Afterward, the cells were incubated for 72 h and treated with or without laser irradiation (808 nm, 1.5 W/cm<sup>2</sup> for 5 min). The cells were then incubated for an additional 24 h. In vitro cytotoxicity was determined using a 3-(4,5-dimethylthiazol-2-yl)-2,5-diphenyltetrazolium bromide (MTT)-based assay.

The Trypan Blue exclusion method was also carried out to detect the viability of the drug-treated cells. Shortly, at 24 h after seeding, the cells were treated with free ICG 10 µg/mL, ICG-BSA-Cur-NPs and BSA-Cur-NPs (equivalently ~10 µg/mL of ICG and ~20 µg/mL of Cur). After 24 h incubation, the media of cells was refreshed before irradiated with or without a laser. After a 72-h incubation period, the cells were collected to stain with trypan blue. The viable cells and dead cells were detected, and the viability was automatically counted by Automated Cell Counter (LUNA-II™, Logos Biosystems, Inc., South Korea).

A LIVE/DEAD™ viability/cytotoxicity kit was applied to visualize the live and dead cells more clearly. N2a cells were seeded on a 4-well-glass slide (Lab-Tek® II Chamber Slide™ system, Sigma Aldrich) at  $4 \times 10^4$  cells/well. After the same procedure of the Trypan Blue assay, cells were incubated for an additional 24 h and then collected to label with live/dead dyes (live cells were stained green with Calcein-AM, while dead ones were stained red with ethidium homodimer-1). Finally, the stained cells were observed by confocal laser scanning microscopy (CLSM) using a Meta LSM510 device (Carl Zeiss) at excitation and emission wavelengths of 494 and 517 nm, respectively, for Calcein-AM and 528 and 617 nm, respectively, for ethidium

homodimer-1. Separately, the cytotoxicity pattern (both necrosis and apoptosis) of (i) PBS, (ii) BSA-Cur-NPs, (iii) free ICG, (iv) ICG-BSA-Cur-NPs was determined by using a FITC-Annexin V/PI staining kit and using a FACS caliber (BD Bioscience Mountain View, CA, USA).

Finally, programmed cell death at the single-cell level was detected by the TUNEL assay using an in situ cell death detection kit (Red TMR; Roche Diagnostics, Mannheim, Germany). The protocol was partly based on one reported previously.<sup>21,38,39</sup> Briefly,  $5 \times 10^4$  cells were seeded onto glass slides in 12-well plates. The cells were treated in the same manner as for the live/dead assay. After being treated with fixation solution (10% formalin) for 45 min and permeabilization solution (0.1% Triton X-100 in 0.1% sodium citrate) for 2 min, the cells were labeled with 50 mL of TUNEL reagent containing terminal deoxynucleotidyl transferase (TdT) at 37°C for 1 h in the dark. The slides with cells were then washed twice with PBS, dried, and stained with 4.6-diamidino-2-phenylindole solution (DAPI) by using antifade mounting medium with DAPI (VECTASHIELD). The apoptosis of cells was visualized by CLSM.

## Uptake of ICG-BSA-Cur-NPs into N2a Cell Spheroid

Three-dimensional N2a cell spheroids were cultured with slight modifications to previous protocols.<sup>21,28,37,39</sup> Briefly, a 12-well plate was coated with 2% (w/v) hot agarose solution in serum-free DMEM containing 1% penicillin/streptomycin (200 µL/well). After forming the solidified agarose coat, 100 µL of the cell suspension containing approximately  $1 \times 10^5$  cells in 10% FBS in DMEM containing cell spheroids was seeded into each well. The cell spheroids were established over 2 days and were then treated with ICG-BSA-Cur-NPs containing 10 µg/mL of ICG followed by a 24-h incubation. After incubation, the spheroids were washed three times with ice-cold PBS and transferred into glass-bottom cell culture disks (20 mm diameter, polystyrene) to be observed by confocal microscopy using the z-stack image collection mode (5 µm step size, ~45 µm in depth).

## In vivo Photothermal Imaging

The in vivo photothermal effect of PBS and drug samples was observed in mice bearing N2a tumors. Each mouse received a subcutaneous injection of 50 µL N2a cell suspension ( $2.5 \times 10^6$  cells). Once the tumor volume reached

~200 mm<sup>3</sup>, 100- $\mu$ L aliquots of PBS or drug samples (2 or 5 mg/kg of body weight of ICG or Cur equivalent, respectively) were injected into the tail vein of the mice. At 6 h post-injection, the mice were irradiated with the laser (808 nm, 1.5 W/cm<sup>2</sup> for 10 min). The temperature changes were recorded and observed by a FLIR E85 photothermal camera (FLIR Systems, Inc., Wilsonville, U.S.A.).

## Antitumor Efficacy of ICG-BSA-NPs in N2a-Tumor-Bearing Mice

Depending on their treatment, mice were divided into five groups: (i) PBS, (ii) BSA-Cur-NPs, (iii) free ICG, (iv) ICG-BSA-Cur-NPs I (mild hyperthermia), and (v) ICG-BSA-Cur-NPs II (hyperthermia). Aliquots (100  $\mu$ L) of PBS or drug samples (2 or 5 mg/kg of body weight of ICG or Cur equivalent, respectively) were injected individually into the mice via the tail vein. At 6 h post-injection, the treated mice were irradiated with a laser (808 nm, 1.5 W/cm<sup>2</sup>) for 10 min with the exception of the mild-hyperthermia group (ICG-BSA-Cur-NPs I), which was irradiated with the temperature limited to a maximum of ~42°C (808 nm, 1.0 W/cm<sup>2</sup>). The tumor volume and the body weight of the treated mice were measured every day for 2 weeks. In the meantime, the histopathology of tumors was evaluated using a previously described procedure.<sup>42,43</sup> Tumors in each group were excised at 24 h post-irradiation. The specimens were then fixed with formalin, embedded in paraffin, sectioned, and stained with hematoxylin and eosin (H&E). The histopathology of the tumors of all groups was compared under a light microscope.

## Data Analysis

Data are presented as the mean  $\pm$  standard deviation (SD). Significant differences were determined using Student's t-tests. P-values <0.05 were considered statistically significant.

## Results

### Preparation and Characterization of BSA-Cur-NPs and ICG-BSA-Cur-NPs

BSA-Cur-NPs and ICG-BSA-Cur-NPs were fabricated using a high-pressure homogenizer based on the nab<sup>TM</sup> technology (Figure 1). The sizes of the prepared BSA-Cur-NPs and ICG-BSA-Cur-NPs were 157.3  $\pm$  17.6 and 158.4  $\pm$  13.7 nm, respectively (Figure 2A). The zeta potentials of the BSA-Cur-NPs and ICG-BSA-Cur-NPs were found to be

-36.3  $\pm$  0.7 and -38.4  $\pm$  2.7 mV, respectively (Figure 2B). The TEM and FE-SEM results revealed that these two NPs were highly uniform and spherical (Figure 2C and D). Overall, both particles were very similar in size, zeta potential and surface morphology. The encapsulation efficiencies of the Cur in BSA-Cur-NPs, ICG-BSA-Cur-NPs and the ICG in ICG-BSA-Cur-NPs were 58.9  $\pm$  6.6%, 73.1  $\pm$  16.5% and 96.7  $\pm$  3.1%, respectively.

### Stability of ICG-BSA-Cur-NPs and Cur/ICG Release from ICG-BSA-Cur-NPs

The stability of the BSA-Cur-NPs and ICG-BSA-Cur-NPs was evaluated over 48 h based on the maintenance of particle size. As shown in Figure 3A, the particle sizes of the BSA-Cur-NPs and ICG-BSA-Cur-NPs were relatively well maintained over this time period. Colloidal dispersions of BSA-Cur-NPs and ICG-BSA-Cur-NPs after reconstitution were approximately the same as they were before lyophilization, indicating good nanoparticle stability (Figure 3B).

The in vitro release profiles of Cur and ICG from BSA-Cur-NPs and ICG-BSA-Cur-NPs were observed over 48 h. Overall, there was a nonsignificant difference between the release behavior of Cur and ICG in both NPs (Figure 3C). From ICG-BSA-Cur-NPs, the ICG release was minutely faster than that of Cur. Cur released from ICG-BSA-Cur-NPs a little faster than from BSA-Cur-NPs. Overall, the release patterns of ICG and Cur were almost identical, and ~70% of both were released from the BSA-NPs after 48 h. Particularly, the concentrations of Cur samples were quantified by fluorescence spectrometry using a calibration curve obtained at 520 nm (emission wavelength), of which stability had carefully been validated by the reversed-phase HPLC assay method (Figure S1 and S2, Supplementary materials).<sup>40</sup> At this wavelength condition, ICG interference was not shown in quantitating Cur because ICG has a peak excitation wavelength of 740–800 nm and peak emission wavelength of 800–860 nm range (data not shown).

### UV-VIS-NIR Absorbance Profile and Photothermal Conversion Activity

The UV-VIS-NIR absorbance spectra of free Cur in acetonitrile, and free ICG, ICG-BSA, BSA-Cur-NPs, and ICG-BSA-Cur-NPs in DW were observed at the wavelength range from 300 to 900 nm. As shown in Figure 4A, the sample groups including ICG (free ICG, ICG-BSA, and ICG-BSA-Cur-NPs) showed significant spectral peaks around 800 nm, which

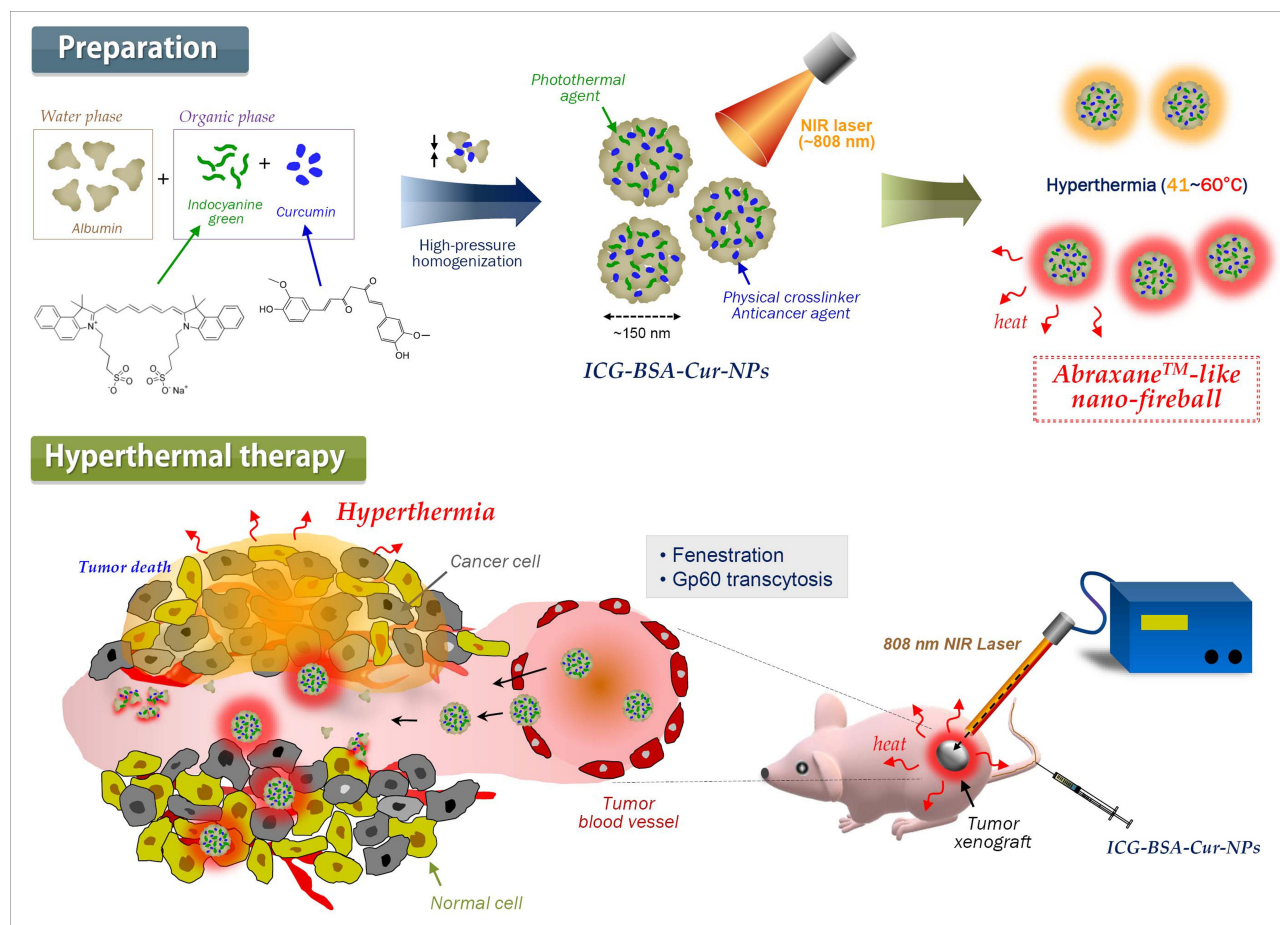


**Figure 1** Schematic of the preparation of ICG-BSA-Cur-NPs and their hyperthermia/targeting-based tumor ablation with NIR laser irradiation.

corresponded to the typical absorbance spectrum of free ICG, whereas spectra of free Cur and BSA-Cur-NPs contained a vast peak in the range of ~400-500 nm without absorption at ~800 nm.

Heat generation is a fundamental parameter for evaluating photothermal efficiency. Among the test groups, only ICG-containing samples strongly absorbed 808 nm-light. This absorption converts photoenergy into thermal energy, damaging surrounding cells via heat. As a result, only ICG-containing samples displayed clear temperature increases in response to the laser irradiation, unlike the BSA-Cur-NPs and PBS samples. Figure 4B indicates the proportional relationship between ICG concentration and the level of heat generation. The temperatures of the ICG-BSA-Cur-NPs with 5, 10, 20  $\mu\text{g}/\text{mL}$  of ICG and the free ~10  $\mu\text{g}/\text{mL}$  ICG reached peak temperatures of 47.6°C, 60.6°C, 71.6°C, and 61.3°C, respectively, within ~5–7 min of laser radiation. However, the temperature of the BSA-Cur-NPs and PBS samples remained steady at around 31°C upon laser irradiation. These clear temperature changes were verified visually by

using a photothermal camera, which shows the strong color intensity of ICG-containing sample groups (Figure 4C).

### Cytotoxicity Evaluations of ICG-BSA-Cur-NPs

Four separate assays were conducted to perform comprehensive cytotoxic evaluations of the samples. MTT results illustrate the dose-dependent cytotoxicity of Cur and ICG with or without laser irradiation (Figure 5A). However, either ICG or Cur-containing (NPs) samples were toxic to N2a cells only at high concentrations (>20  $\mu\text{g}/\text{mL}$  for both ICG and Cur) without laser irradiation. The ICG-BSA-Cur-NPs effectively killed N2a cells even at a low concentration (~0.3  $\mu\text{g}/\text{mL}$ ) in response to 808 nm-laser irradiation, and their inhibitory concentration ( $\text{IC}_{50}$ ) values were shown to be much less than 0.3  $\mu\text{g}/\text{mL}$ . No critical cytotoxicity change was found for the BSA-Cur-NPs with laser irradiation.

In the live/dead assay, almost all cells seemed to be killed after treatment with free ICG (~10  $\mu\text{g}/\text{mL}$ ) and ICG-BSA-Cur

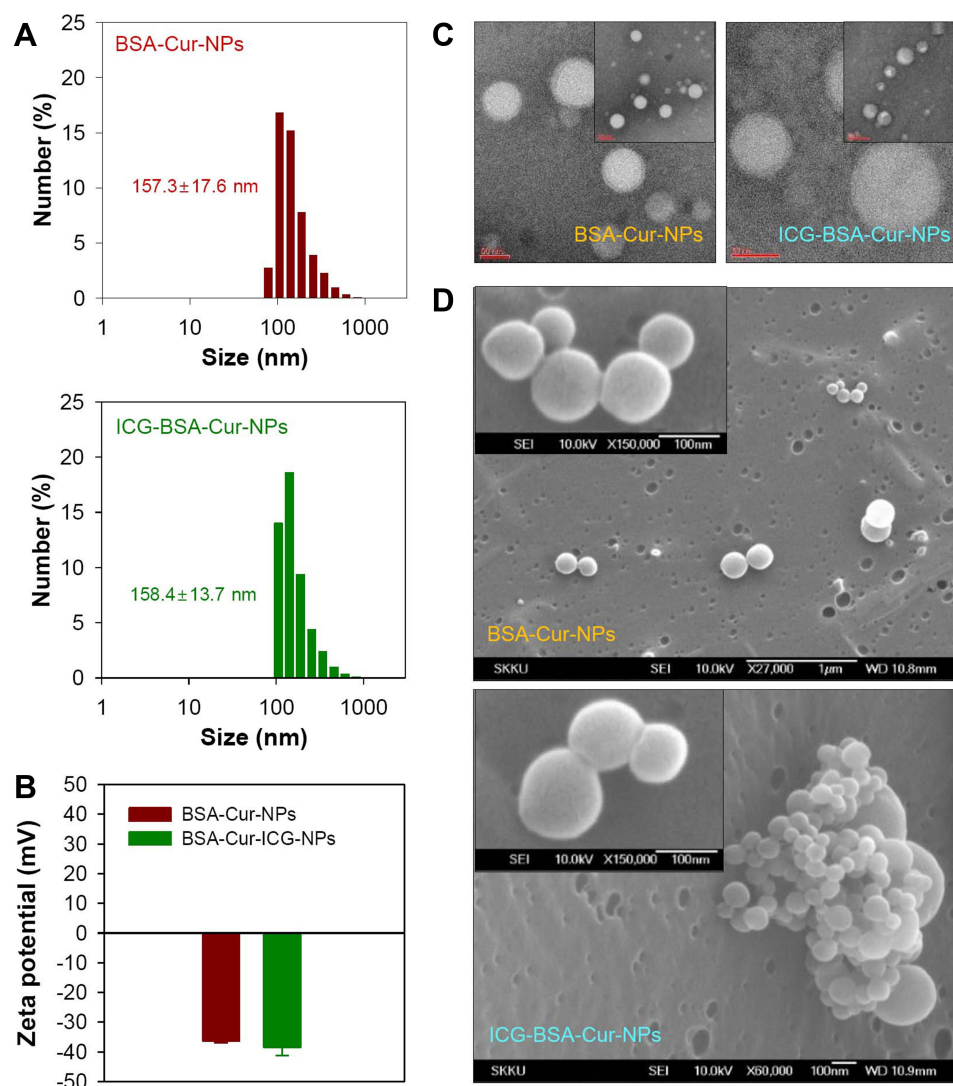


**Figure 2** Histograms of (A) particle size and (B) zeta potential of BSA-Cur-NPs and ICG-BSA-Cur-NPs. (C) TEM and (D) FE-SEM images of BSA-Cur-NPs and ICG-BSA-Cur-NPs.

-NPs (~10  $\mu\text{g}/\text{mL}$ ) followed by 808-nm laser irradiation, as visualized by red staining. However, both groups without laser irradiation did not show significant N2a cell death. In contrast, N2a cells treated with PBS were viable as visualized by green staining regardless of laser irradiation. The BSA-Cur-NPs treatment resulted in partial cell death, as indicated by red signal, and partial viability, as indicated by green signal, regardless of laser irradiation. This result seemed to reflect the inherent cytotoxic effect of curcumin at high concentration (Figure 5B). In Trypan blue assay, the viability of cells was calculated automatically by using the Automated Cell Counter. Notably, only ~5% of cells treated with ICG-BSA-Cur-NPs exposed to a laser were viable (Figure 5C and D).

The TUNEL assay reveals the morphology of dead or live cells at the single-cell level. The fluorescence of Cur

(yellow signal; both laser (-) and laser (+)) indicates the internalization of BSA-Cur-NPs and ICG-BSA-Cur-NPs. Additionally, the TUNEL fluorescence (red signal) of ICG-BSA-Cur-NPs or free ICG resulted in cell death due to thermal or/and chemotherapeutic effects, generating apoptotic cells or bodies (Figure 6A).

FACS analysis results also illustrated the progress of cell apoptosis induced by free ICG, BSA-Cur-NPs, ICG-BSA-Cur-NPs. At our experimental settings (808-nm laser irradiation and 72 h incubation), almost all cells incubated with ICG-BSA-Cur-NPs, similar with free ICG, were shown to be dead via apoptosis, while less than 80% of BSA-Cur-NPs group were dead by this mechanism (Figure 6B). This fact indicated that the increased temperature stress might facilitate the apoptosis of N2a cells.

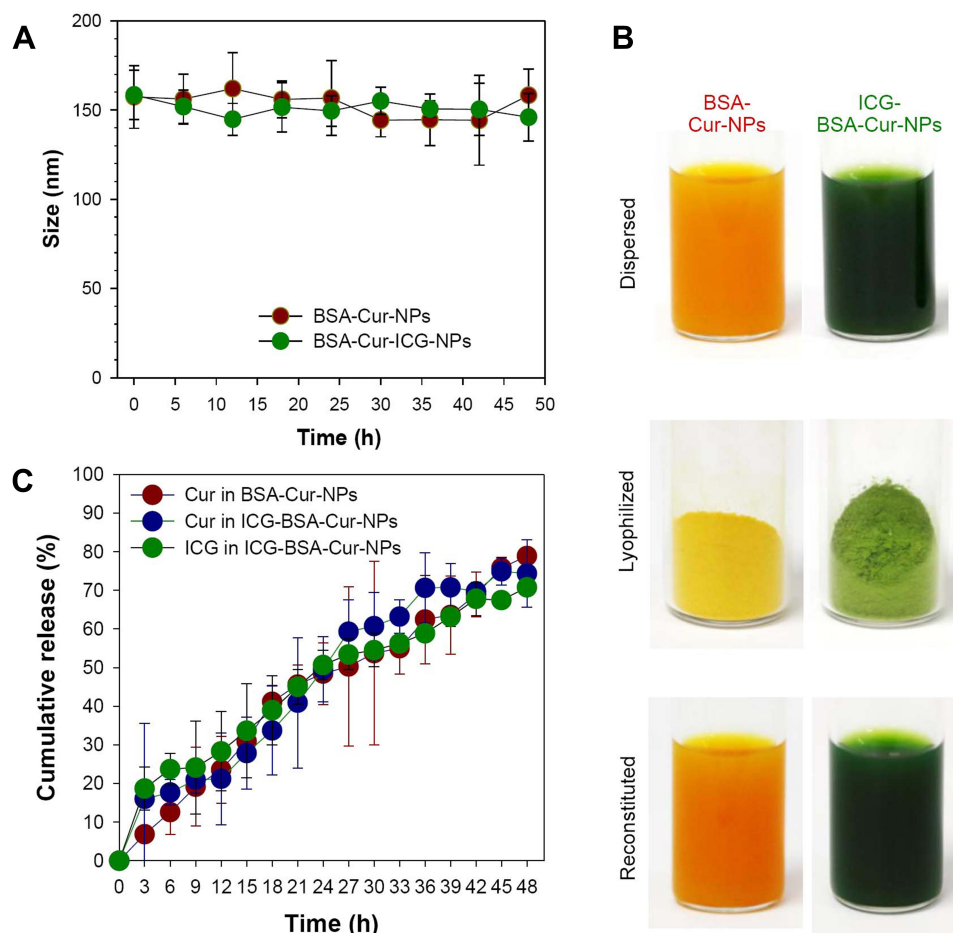


**Figure 3** (A) Physical stability of BSA-Cur-NPs and ICG-BSA-Cur-NPs based on size changes over 48 h. (B) Photographs of the solution (top), lyophilized powder (middle), and reconstituted suspension (bottom) of the BSA-Cur-NPs and ICG-BSA-Cur-NPs. (C) Release profile of Cur and ICG from the NPs.

## Uptake of ICG-BSA-Cur-NPs into N2a Cell Spheroids

Uptake of ICG-BSA-Cur-NPs into N2a cell spheroids was observed by CLSM. Spheroids are considered to be an *in vitro* model system of tumors that mimic three-dimensional tumor tissues *in vivo*.<sup>44</sup> N2a cell spheroids were incubated with ICG-BSA-Cur-NPs for 24 h. The confocal spectroscopic images of N2a cell spheroids obtained from slices with a 5- $\mu$ m step size showed clear red and yellow fluorescence, indicating that both ICG and Cur were internalized into the spheroids (Figure 7A). These results might imply that ICG-BSA-Cur-NPs would be able to permeate into three-dimensional tumor tissues *in vivo*.

## Hyperthermia and Tumor Localization of ICG-BSA-Cur-NPs in N2a Tumor-Bearing Mice

ICG-BSA-Cur-NPs were highly localized in the tumors of N2a cell-xenografted mice (Figure 7B and C). When

visualized with a thermal imaging camera, the local tumor temperatures of mice injected with ICG-BSA-Cur-NPs increased to  $\sim 55^{\circ}\text{C}$  after 5 min of NIR irradiation at 808 nm, which is considered to be sufficient for a hyperthermal antitumor therapy as this is a lethal temperature for most cancer cells. In contrast, the local tumor temperatures of the mice treated with BSA-Cur-NPs and PBS incremented marginally (from  $35^{\circ}\text{C}$  to  $\sim 41^{\circ}\text{C}$ ) due to well-controlled laser irradiation (Figure 7B).

## Antitumor Efficacy of ICG-BSA-Cur-NPs in N2a Tumor-Bearing Mice

The antitumor effects of ICG-BSA-Cur-NPs and control groups were evaluated in N2a tumor-bearing mice. The tumor volumes of mice were measured over 14 days after treatment (Figure 8A). The final tumor volumes for the PBS, BSA-Cur-NPs, free ICG, ICG-BSA-Cur-NPs I (mild hyperthermia:  $41\sim 42^{\circ}\text{C}$ ), and ICG-BSA-Cur-NPs II

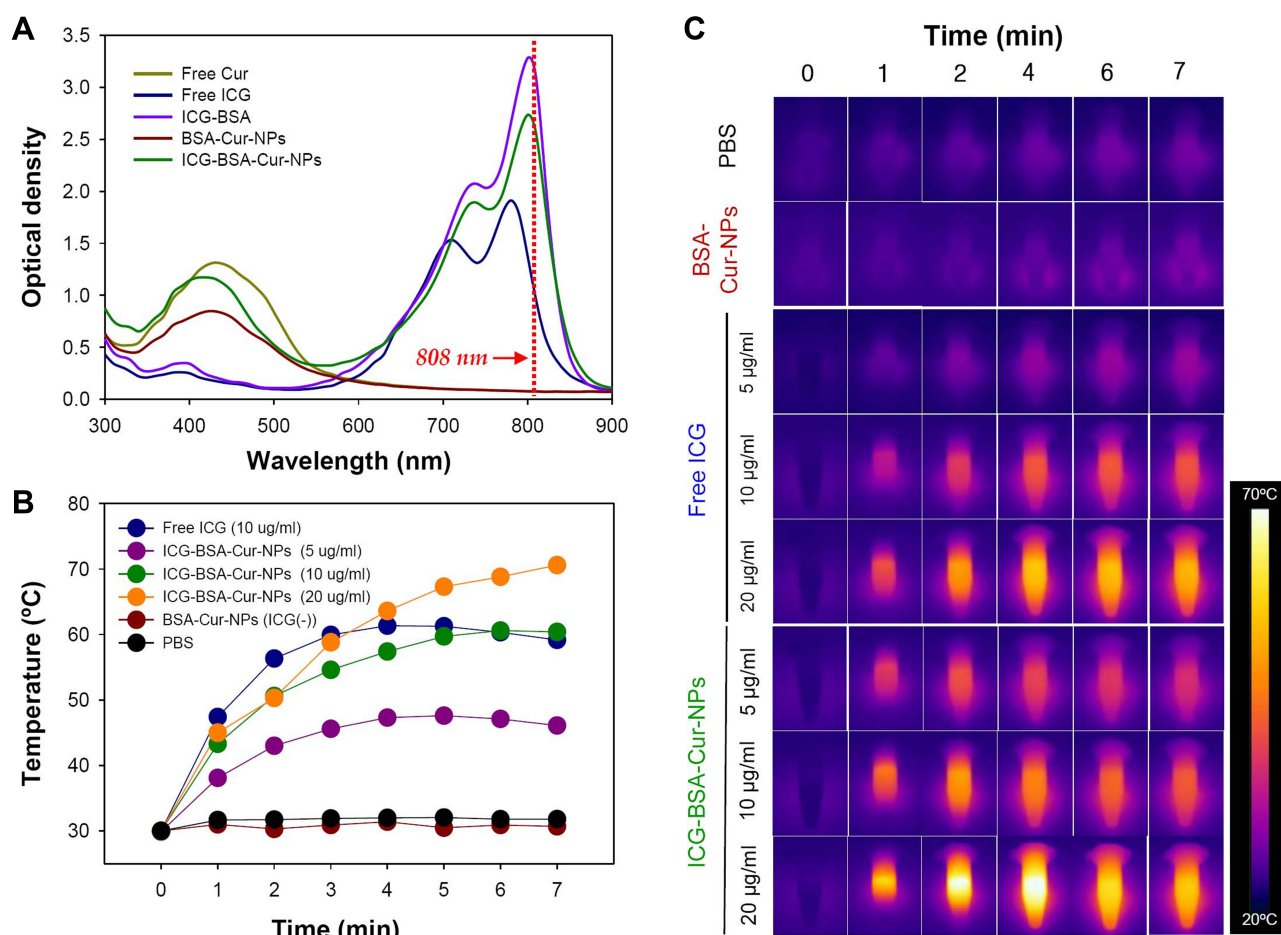


**Figure 4** (A) UV-Vis-NIR absorption spectra of free Cur, free ICG, ICG-BSA, BSA-Cur-NPs, and ICG-BSA-Cur-NPs. (B) Surface temperature profiles of PBS, free ICG and ICG-BSA-Cur-NPs with different ICG concentrations (5, 10 and 20 µg/mL) over 7 min, upon NIR laser irradiation (808 nm, 1.5 W/cm<sup>2</sup>). (C) Thermographic images of PBS, BSA-Cur-NPs (without ICG), free ICG and ICG-BSA-Cur-NPs with different ICG concentrations (5, 10 and 20 µg/mL) after NIR laser irradiation (808 nm, 1.5 W/cm<sup>2</sup>).

(hyperthermia: no limit) groups were  $1408.6 \pm 551.9$ ,  $1190.6 \pm 343.6$ ,  $888.6 \pm 566.2$ ,  $1047.5 \pm 248.6$ , and  $103.0 \pm 111.3$  mm<sup>3</sup>, respectively. Notably, tumor growth in mice treated with ICG-BSA-Cur-NPs II was greatly suppressed, and the resulting averaged tumor size was ~13- and 8-fold smaller than those of the PBS and free ICG controls, respectively (Figure 8B and C).

Furthermore, the treatment response of tumors is directly proportional to cell density and color intensity of H&E-stained tumor sections and the surface morphology of the tumor after treatment. After laser irradiation, the tumor surface of mice treated with ICG-contained NPs became much darker than those of the other treatment groups, indicating a significantly stronger response to treatment. As shown in Figure 8C (right), photographic images of H&E-stained tumor sections from control groups showed regular N2a cell growth patterns, while that of the ICG-BSA-Cur-NPs group displayed much weaker staining, showing a remarkable decrease in tumor

cell death. Nonetheless, the weight of the mice in all treatment groups remained quite stable over 14 days, indicating that the mice were cared for well (Figure 8D).

## Discussion

In a clinical setting, hyperthermia is used as a therapeutic procedure to increase the temperature of a specific region of the body affected by cancer.<sup>45</sup> Mild hyperthermia around 41–42°C plays a role in enhancing the delivery of anticancer drugs to tumors by increasing blood flow and improving the vascular permeability in tumors.<sup>46</sup> Also, it enhances oxygen delivery to tumor tissues and attenuates the tumor hypoxic state.<sup>47</sup> Hyperthermia from 41–42°C to 48°C induces direct cell-killing through irreversible damage at long exposures or through increased susceptibility to radiation and chemotherapy.<sup>45,48</sup> Severe hyperthermia over 48°C results in irreversible damage and denaturation after a few minutes. Likewise,

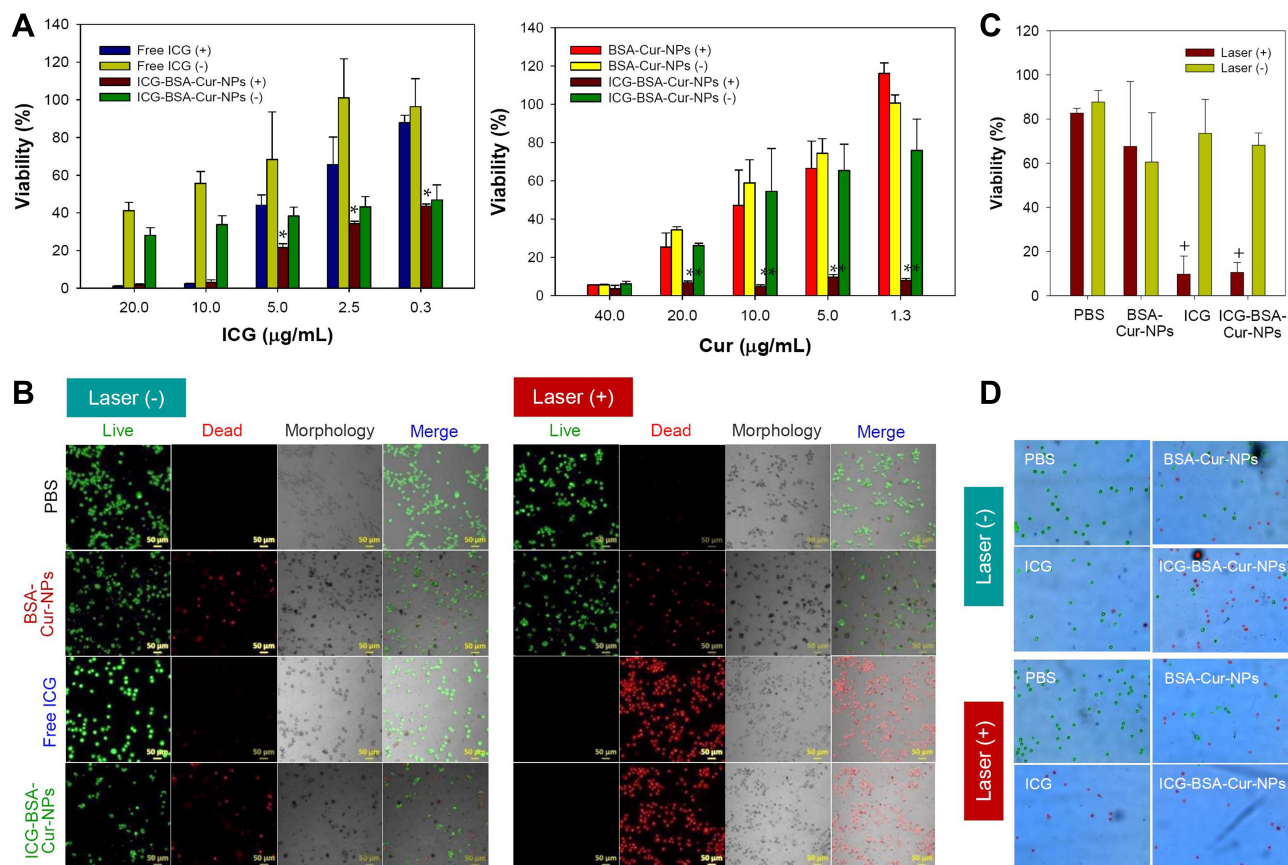


**Figure 5** (A) Cytotoxicity of ICG with 0, 0.3, 2.5, 5, 10, 20 µg/mL Cur (left); and of Cur with 0, 1.3, 5, 10, 20, 40 µg/mL and 10 µg/mL ICG (right) in BSA-Cur-NPs and ICG-BSA-Cur-NPs to N2a cells with or without laser irradiation (808 nm, 1.5 W/cm<sup>2</sup> for 5 min) as evaluated by MTT assay. (B) Live/dead assay of N2a cells incubated with PBS, free ICG, BSA-Cur-NPs and ICG-BSA-Cur-NPs with or without laser irradiation (808 nm, 1.5 W/cm<sup>2</sup> for 10 min). (C) Trypan blue assay-based viability for PBS, free ICG, BSA-Cur-NPs and ICG-BSA-Cur-NPs at fixed concentrations of 20 and 10 µg/mL for Cur and ICG, respectively, with or without laser irradiation (808 nm, 1.5 W/cm<sup>2</sup> for 10 min). (D) Trypan blue-based Live/dead assay of N2a cells incubated with PBS, free ICG, BSA-Cur-NPs and ICG-BSA-Cur-NPs under the same conditions of (C). \**P* < 0.003 over free ICG(+); \*\**P* < 0.001 over all other groups; and \**P* < 0.001 over all other groups.

temperature-controlled hyperthermia can be utilized for the different purpose of anticancer therapy.

The first aim of this study was to concurrently incorporate ICG and Cur in ABX-like albumin nanoparticles. Despite the many advantages of ICG as an FDA-approved theranostic agent, it has a very short circulating half-life of ~34 min because it is very rapidly extracted by the liver. This limited circulation time restricts satisfactory hyperthermal/bioimaging efficacy *in vivo*.<sup>49,50</sup> ICG incorporated in nanoparticles has been shown to exhibit significantly increased circulation time and delivery to tumors.<sup>17,18,51-53</sup> Moreover, despite its high aqueous solubility, ICG strongly binds to albumin and is facily encapsulated into albumin nanoparticles.<sup>13,17</sup> Many studies have reported strong non-covalent interaction between the aromatic and heteroaromatic rings of ICG and the hydrophobic sites of albumin, resulting in the exploitation of unique albumin-based nano-systems.<sup>13,54,55</sup> Likewise, ABX-like

albumin nanoparticles are considered to be a promising formulation platform to improve the many challenging problems with Cur, such as poor aqueous stability *in vitro* and short half-life in blood circulation.<sup>20,26,40</sup> Moreover, Cur is an excellent physical cross-linker that can connect the hydrophobic pockets in albumin molecules for nanoparticle formation due to its hydrophobicity-based affinity and identical left-right symmetric structure. Cur is also a potential natural chemopreventive/chemotherapeutic agent.<sup>40</sup> Based on these characteristics Nab<sup>TM</sup> technology, our ICG-BSA-Cur-NPs were viewed as an attractive platform not only to overcome the limitations of ICG and Cur but also to take advantage of the ICG/Cur synergistic efficacy in the context of combined photothermal chemotherapy.

In our nano-system, the physical interactions among ICG, albumin and Cur were enhanced by the high-pressure homogenization process, which formed ~150-nm spherical

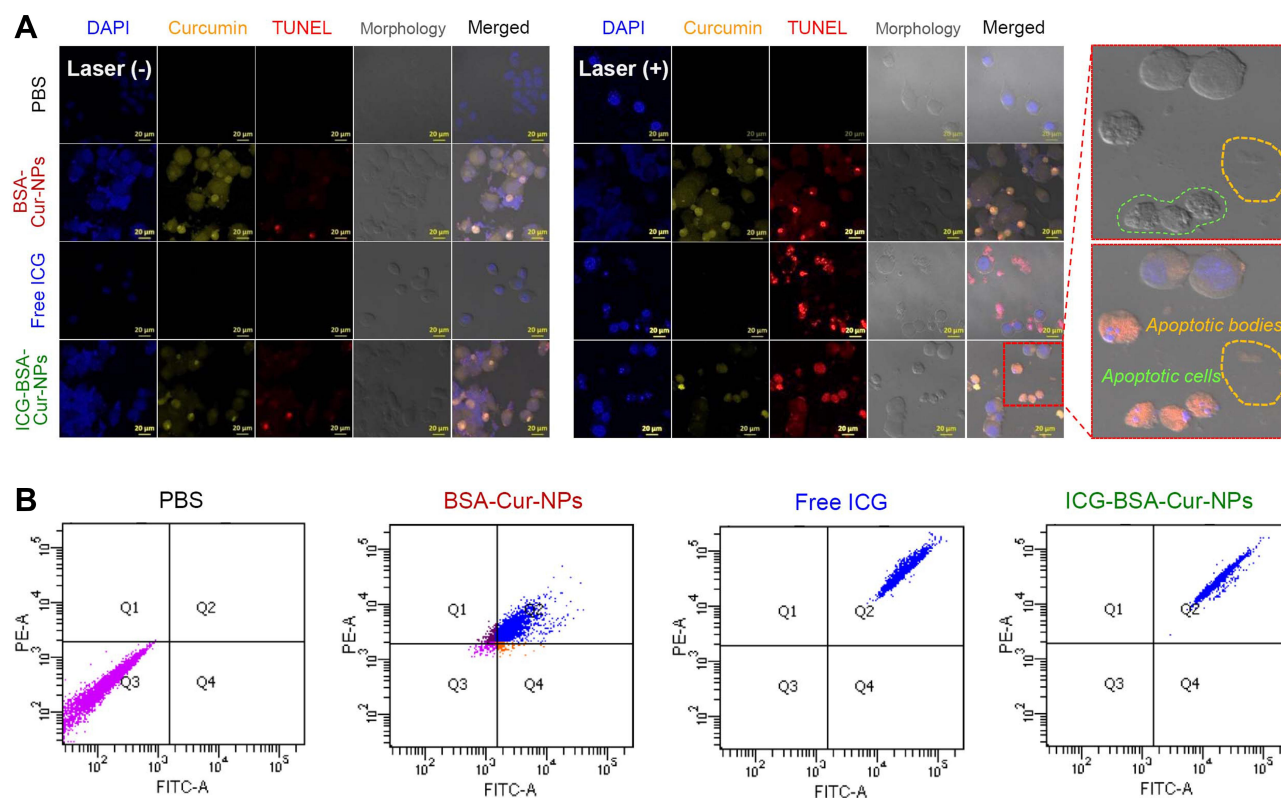


**Figure 6** (A) Cytotoxicity evaluation based on TUNEL assay of N2a cells incubated PBS, free ICG, BSA-Cur-NPs and ICG-BSA-Cur-NPs with or without laser irradiation (808 nm, 1.5 W/cm<sup>2</sup> for 10 min). (B) Flow cytometric analysis of N2a cells incubated with PBS, BSA-Cur-NPs, free ICG and ICG-BSA-Cur-NPs with or without laser irradiation (808 nm, 1.5 W/cm<sup>2</sup> for 10 min). N2a cells were stained by Annexin-V-FITC and propidium iodide (PI).

ICG-BSA-Cur-NPs (Figure 2A and C). ICG-BSA-Cur-NPs were relatively stable at room temperature over 48 h with little change in particle size and appeared to gradually release both ICG and Cur. This release pattern seems to be primarily due to the tight binding of ICG and Cur to BSA (Figure 3A and C). However, the actual release from ICG-BSA-Cur-NPs is expected to be much faster in blood circulation because the nab<sup>TM</sup>-based system tends to break into smaller particles (~10 nm) *in vivo*, which accelerates drug release.<sup>56</sup> The VIS-UV-NIR spectra of free ICG and ICG-containing samples (including ICG-BSA-Cur-NPs) displayed peaks at ~800 nm that is typical of ICG (Figure 4A). Therefore, our ICG-BSA-Cur-NPs responded to 808-nm laser light, resulting in a significant temperature increase during laser irradiation at this wavelength (Figure 4B and C). Additionally, ICG-BSA-Cur-NPs seem to be qualified as a pharmaceutical because they are highly dispersible, well lyophilized, and easily reconstituted, which satisfies the essential characteristics for pharmaceutical manufacturing.

The second aim of this study was to evaluate the cytotoxic effect of ICG-BSA-Cur-NPs on N2a cells using

various assays. When irradiated with 808-nm laser light, ICG-BSA-Cur-NPs were highly toxic to N2a cells at all ICG concentrations, irrespective of Cur concentrations. Cells treated with BSA-Cur-NPs at 20 µg/mL displayed a >60% cytotoxic effect with or without 808-nm laser irradiation (Figure 5B). The IC<sub>50</sub> values of Cur were found to be 30.4 and 14.7 µM (11.1 and 5.4 µg/mL, respectively) for HCT116 and Mia PaCa2 cells, respectively. These values are significant in that they indicate a mild degree of antitumor effect. Noticeably, the mechanism of cell death was observed in detail at a singular cell level using the TUNEL assay. In this assay, strong red fluorescence indicates DNA strand breaks labelled by TMR red-modified terminal deoxynucleotidyl transferase (TdT), which implicates apoptosis-based cell death and is distinguished from the morphology/colorlessness of normal cells. When treated with ICG-BSA-Cur-NPs followed by 808-nm laser irradiation, the N2a cell shrinkage and blebbing membrane mosaiced with rounded, condensed bodies (that look like early apoptotic bodies) (Figure 6A). Such features resemble the changes in morphologic hallmarks during the apoptotic process. Thus, this observation is consistent with

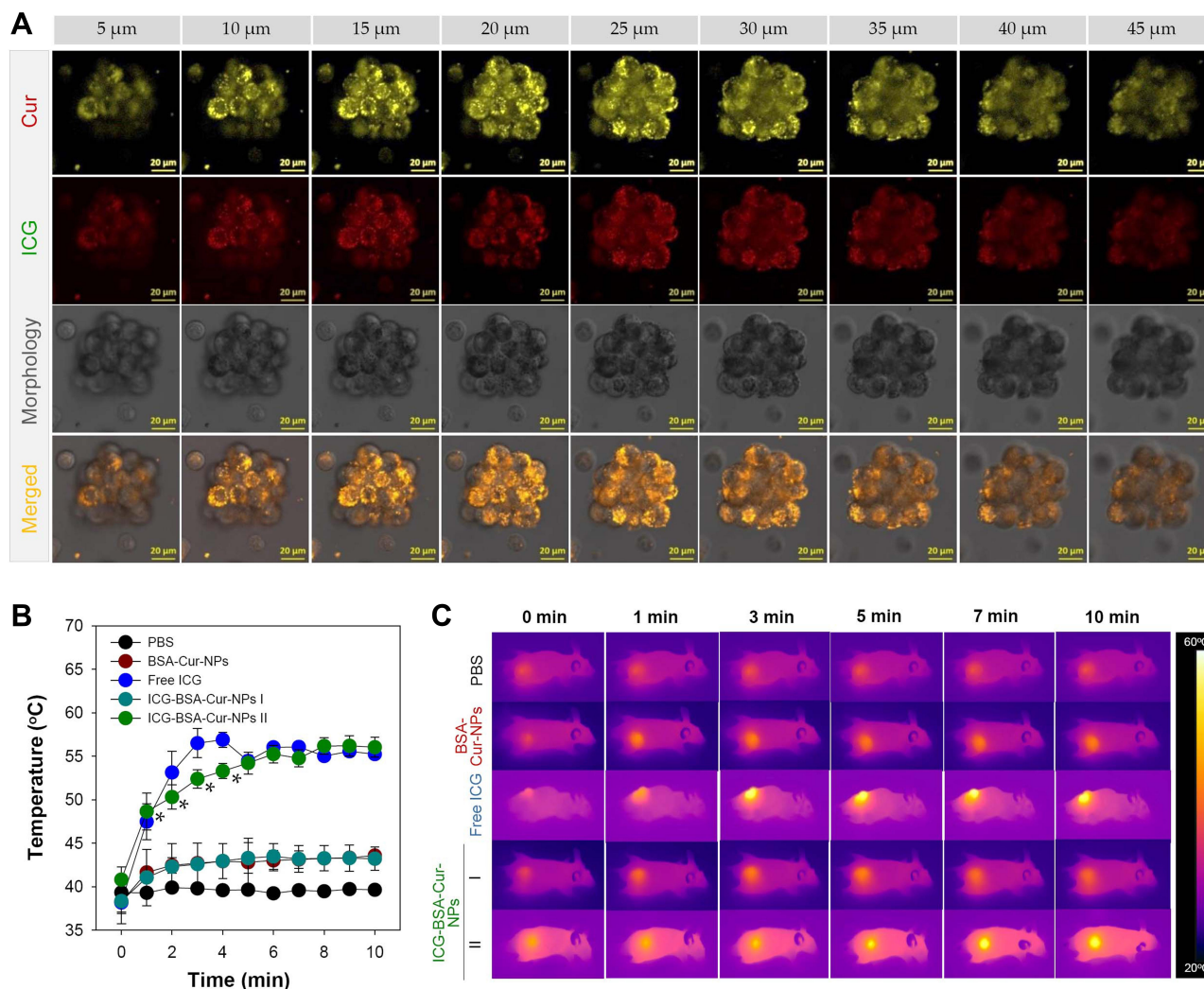


**Figure 7** (A) Permeability of ICG-BSA-Cur-NPs into N2a cell spheroids. Spheroids were treated with ICG-BSA-Cur-NPs (ICG~10  $\mu\text{g}/\text{mL}$ ) and z-stack images of nine 5- $\mu\text{m}$  slices were obtained for each Cur and ICG. (B) In vivo monitoring of hyperthermal localization of BSA-Cur-NPs and ICG-BSA-Cur-NPs with laser irradiation (808 nm, 1.0 and 1.5  $\text{W}/\text{cm}^2$  for 10 min) in N2a tumor-bearing mice. Mild hyperthermia caused by ICG-BSA-Cur-NPs was conducted using a laser power of 1.0  $\text{W}/\text{cm}^2$  with temperature increase limited to a maximum of  $\sim 41.42^\circ\text{C}$  (I). (C) Thermographic images of N2a tumor-bearing mice during laser treatment. \* $P < 0.01$  over BSA-Cur-NPs and ICG-BSA-Cur-NPs I.

the previous results that Cur induces apoptosis.<sup>17</sup> Moreover, ICG-BSA-Cur-NPs were able to penetrate deep inside the 3D N2a cell structure ( $\sim 30 \mu\text{m}$ ), as indicated by the yellow and red fluorescence colors of Cur and ICG, respectively. These results provide potential evidence of the passive targetability of our nanoparticles in an in vivo tumor-mimicking environment.

The final aim of this study was to assess the antitumor effect of ICG-BSA-Cur-NPs in N2a cell-xenograft animals. As mentioned previously, the mice treated with ICG-BSA-Cur-NPs were divided into two different groups that were subjected to mild-hyperthermia (I) and hyperthermia (II). The tumor temperature of the mild-hyperthermia mice group was limited to temperatures below  $\sim 42^\circ\text{C}$  with low-intensity laser

irradiation. However, only marginal antitumor efficacy was observed in this ICG-BSA-Cur-NPs I group due to the low dose of Cur ( $\sim 5 \text{ mg Cur}/\text{kg body}$ ) as apoptosis was based on dose-dependent induction by Cur in this case. The resulting low plasma or tumor level of Cur seemed to be below the threshold that would fully suppress tumor growth in mice. Nevertheless, this mild hyperthermia is meaningful because it causes the blood vessels to dilate and to be more permeable, enabling increased nanoparticle accumulation in the irradiated tumor area. Mild hyperthermia also augments the permeability of nanoparticles into the cell membrane and/or enhances endocytosis.<sup>10–13</sup> Subsequently, a higher Cur dose or replacement with more potent agents in our system might be required for better antitumor efficacy in this system.

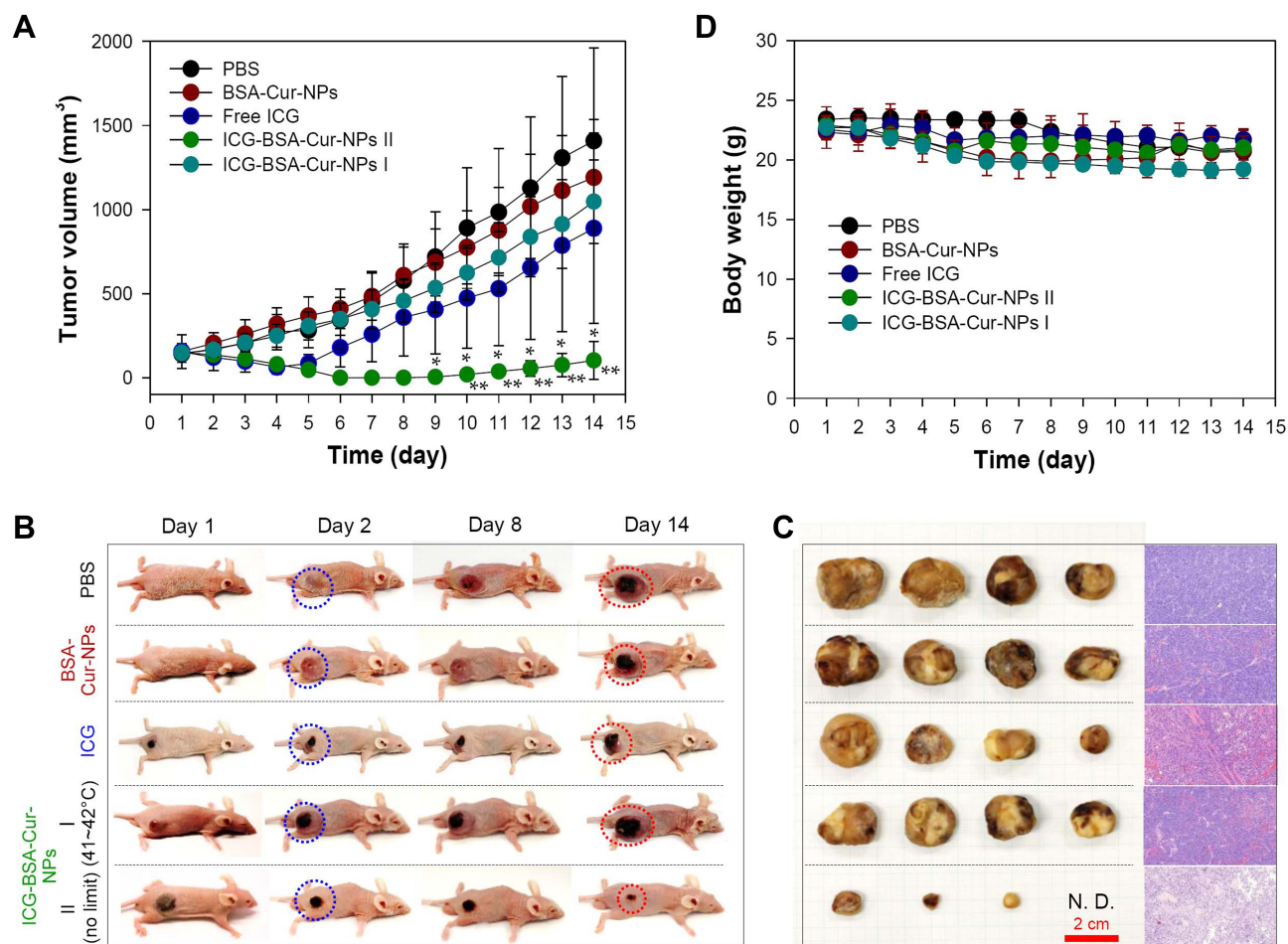


**Figure 8** In vivo antitumor efficacy of PBS, free ICG, BSA-Cur-NPs and ICG-BSA-Cur-NPs groups I and II. **(A)** Profiles for tumor growth of N2a tumor-bearing mice using laser powers of 1.0 and 1.5 W/cm<sup>2</sup>. \* $P < 0.001$  over all groups except ICG and \*\* $P < 0.01$  over free ICG. **(B)** Representative photographs of N2a tumor-bearing mice at 1, 2, 8 and 14 days after treatment. **(C)** Photographs of tumors excised from each group and H&E-stained tumor tissues of each group at 24 h post-treatment (right). **(D)** Body weight change of N2a tumor-bearing mice in the different treatment groups over 14 days post-treatment.

On the other hand, the full hyperthermia group, ICG-BSA-Cur-NPs II, was exposed to unlimited laser irradiation, resulting in complete ablation of the xenografted N2a tumors until day 9. This was due to the combined effect of hyperthermia-based apoptosis by ICG and enhanced delivery of Cur to tumors. Thermal ablation is more promising if it minimizes residual tumor tissue which causes tumor recurrence.<sup>57,58</sup> Consistent with this fact, the tumor volume of mice treated with free ICG relapsed very quickly after thermal ablation. Combining thermal ablation with adjuvant chemotherapeutics might address this problem. In the central zone of laser irradiation, tumor tissue undergoes complete heat-ablation (necrosis is often predominant due to the extreme conditions). In the peripheral and transitional zone of sublethal hyperthermia, incomplete apoptosis or reversible injury to the relevant tumors can be enhanced by the additional cytotoxic effect of chemotherapeutic

agents.<sup>59</sup> Despite excellent initial tumor ablation, a slight rebound of tumor volume of mice group ICG-BSA-Cur-NPs II was observed on day 10, which might be explained by incomplete hyperthermic removal or low effective Cur dose. This result suggests that the next step in studying the combined therapy of hyperthermal ablation and chemotherapeutics is to optimize dosing.

Finally, the nanoparticle size is of paramount importance for nanocarrier to cross blood-brain barrier (BBB). In this study, we chose the glioblastoma N2a cell-xenograft tumor model to identify the antitumor efficacy of ICG-BSA-Cur-NPs, but which does not reflect the biological environment of BBB that hardly allows penetration of nanoparticles and other hydrophilic drugs. In general, the size 200 nm is estimated as a limiting size for nanoparticles to undergo endocytosis through a clathrin-mediated mechanism, so less than 200 nm have more chances to cross the BBB,<sup>60</sup> and most efficiently,

nanoparticles of <20 nm.<sup>61,62</sup> Despite the original size of ~150 nm, the in vivo behavior of our ABX-like albumin NPs (ICG-BSA-Cur-NPs) seems amenable to tumor targeting and crossing BBB because the ABX quickly dissociates, breaking into smaller fragments (~10 nm) in the blood, despite their original sizes of ~130 nm.<sup>56,63-66</sup> These smaller fragments are mostly albumin-bound paclitaxel complexes (94%), and a small fraction of unbound paclitaxel (6%).<sup>67</sup> Prepared by using the Nab<sup>TM</sup>-based technique, our NPs are expected to have the similar in vivo behavior with ABX. The mechanism of how our NPs quickly dissociate into small albumin-bound-hydrophobic-drug units is hypothesized based on the mechanism of how the NPs formed and the dynamic and chaotic blood circulation in the body. Furthermore, these albumin-bound units (~10 nm) are expected to be more favorable to their transport across BBB to brain tumors.<sup>60-62</sup> More importantly, the albumin receptors (gp60 and SPARC) are expressed in many solid tumors including brain tumor actively target the albumin-bound drug to accumulate in. Lin developed the blood-brain-barrier-penetrating albumin NPs (~150 nm in size) for biomimetic drug delivery via albumin-binding protein pathways for anti-glioma therapy and reported the dual roles of albumin in the nano-system.<sup>36</sup> As with ABX and other albumin NPs, our ICG-BSA-Cur-NPs are believed to dissociate to ~10 nm-albumin-bound units in plasma and presumably cross the BBB via gp60-mediated endothelial endocytosis, showing superior tumor targetability vs others in clinical settings.

In addition, albumin molecule itself is a significant dysopsonin that prevents the adsorption of a variety of plasma proteins and macrophage recognition, which extends the circulating time of nanoparticles made of albumin. So, albumin precoating onto nanoparticle surface is used as one of the good approaches to improve blood circulation and reduce hepatic uptake clearance.<sup>29,30</sup> Likewise, the Nab<sup>TM</sup> technique is barely affected by the plasma protein adsorption or corona layer formation in terms of pharmacokinetic modulation. This fact might increase the probability that our ICG-BSA-Cur-NPs, as either whole particles or dissociated fragments, would prevent glomerular filtration and protein corona formation, which facilitates blood clearance of ICG as well as Cur. We believe that this pharmacokinetic extension would be another clinical advantage in terms of improved antitumor therapy.

The skull can be a practical hurdle that ruins the efficiency of photothermal therapy. The deep red NIR laser (650~900 nm) is hard to reach the brain tumor sites across the skull due to its penetration limitation (2~3 mm

depth). Actually, this clinical restriction seems common with almost all tumors that are deeply located in the body, except some grown on the skin. Thus, the application of our ICG-BSA-Cur-NPs should be carefully maneuvered by using a brand-new injection-type NIR-emitting probe in an orthotopic brain tumor model in the near future.

## Conclusion

In conclusion, we introduced the nano-fireball-like albumin nano-platform encapsulating both indocyanine green and curcumin. Our Nab<sup>TM</sup> technology-based ABX-like ICG-BSA-Cur-NPs of ~150 nm in size displayed strong hyperthermal response to 808-nm NIR light and acceptable physicochemical characteristics. Based on the hyperthermia-induced anticancer effect in vitro and in vivo, our study demonstrated that ICG-BSA-Cur-NPs were able to ablate the N2a cell-based tumor xenografts. Additionally, ICG-BSA-Cur-NPs showed better antitumor effect under mild hyperthermia (41~42°C) vs the monotherapy of BSA-Cur-NPs, but the overall suppression was not highly remarkable due to moderate cytotoxicity of curcumin. This is remained for a further study of potent chemotherapeutic albumin nanoparticles accompanied by mild hyperthermia. We believe that ICG-BSA-Cur-NPs would be potentially used as a future brain tumor treatment.

## Funding

This work was supported by the National Research Foundation of Korea (NRF) grants funded by the Korea government (MSIT) (No. NRF-2019R1A2C2085292 and No. NRF-2019R1A5A2027340).

## Disclosure

The authors have no conflicts of interest to declare for this work.

## References

1. Zhang Z, Wang J, Chen C. Near-infrared light-mediated nanoplatforams for cancer thermo-chemotherapy and optical imaging. *Adv Mater.* 2013;25(28):3869-3880. doi:10.1002/adma.201301890
2. Park S, Kim H, Lim SC, et al. Gold nanocluster-loaded hybrid albumin nanoparticles with fluorescence-based optical visualization and photothermal conversion for tumor detection/ablation. *J Control Release.* 2019;304:7-18. doi:10.1016/j.jconrel.2019.04.036
3. Seo B, Lim K, Kim SS, et al. Small gold nanorods-loaded hybrid albumin nanoparticles with high photothermal efficacy for tumor ablation. *Colloids Surf B Biointerfaces.* 2019;179:340-351. doi:10.1016/j.colsurfb.2019.03.068

4. Zhang XD, Wu D, Shen X, et al. Size-dependent in vivo toxicity of PEG-coated gold nanoparticles. *Int J Nanomed.* 2011;6:2071–2081. doi:10.2147/IJN.S21657
5. Song X, Chen Q, Liu Z. Recent advances in the development of organic photothermal nano-agents. *Nano Res.* 2015;8(2):340–354. doi:10.1007/s12274-014-0620-y
6. Cai H, Ma Y, Wu Z, et al. Protein corona influences liver accumulation and hepatotoxicity of gold nanorods. *Nano Impact.* 2016;3:40–46. doi:10.1016/j.impact.2016.09.005
7. Hauck TS, Jennings TL, Yatsenko T, Kumaradas JC, Chan WC. Enhancing the toxicity of cancer chemotherapeutics with gold nanorod hyperthermia. *Adv Mater.* 2008;20(20):3832–3838. doi:10.1002/adma.200800921
8. Park H, Yang J, Lee J, Haam S, Choi IH, Yoo KH. Multifunctional nanoparticles for combined doxorubicin and photothermal treatments. *ACS Nano.* 2009;3(10):2919–2926. doi:10.1021/nn900215k
9. Chen H, Di Y, Chen D, et al. Combined chemo-and photo-thermal therapy delivered by multifunctional theranostic gold nanorod-loaded microcapsules. *Nanoscale.* 2015;7(19):8884–8897. doi:10.1039/C5NR00473J
10. Sherlock SP, Tabakman SM, Xie L, Dai H. Photothermally enhanced drug delivery by ultrasmall multifunctional FeCo/graphitic shell nanocrystals. *ACS Nano.* 2011;5(2):1505–1512. doi:10.1021/nn103415x
11. Tian B, Wang C, Zhang S, Feng L, Liu Z. Photothermally enhanced photodynamic therapy delivered by nano-graphene oxide. *ACS Nano.* 2011;5(9):7000–7009. doi:10.1021/nn201560b
12. Wang C, Xu H, Liang C, et al. Iron oxide@ polypyrrole nanoparticles as a multifunctional drug carrier for remotely controlled cancer therapy with synergistic antitumor effect. *ACS Nano.* 2013;7(8):6782–6795. doi:10.1021/nn4017179
13. Chen Q, Liang C, Wang C, Liu Z. An imagable and photothermal “Abraxane-like” nanodrug for combination cancer therapy to treat subcutaneous and metastatic breast tumors. *Adv Mater.* 2015;27(5):903–910. doi:10.1002/adma.201404308
14. Frangioni JV. In vivo near-infrared fluorescence imaging. *Curr Opin Chem Biol.* 2003;7(5):626–634. doi:10.1016/j.cbpa.2003.08.007
15. Yannuzzi LA. Indocyanine green angiography: a perspective on use in the clinical setting. *Am J Ophthalmol.* 2011;151(5):745–751.e1. doi:10.1016/j.ajo.2011.01.043
16. Maryam P, Gianluca P, Nasim C, Abbas B. Dual wavelength irradiation antimicrobial photodynamic therapy using indocyanine green and metformin doped with nano-curcumin as an efficient adjunctive endodontic treatment modality. *Photodiagnosis Photodyn Ther.* 2020;29:101628. doi:10.1016/j.pdpdt.2019.101628
17. Sheng Z, Hu D, Zheng M, et al. Smart human serum albumin-indocyanine green nanoparticles generated by programmed assembly for dual-modal imaging-guided cancer synergistic phototherapy. *ACS Nano.* 2014;8(12):12310–12322. doi:10.1021/nn5062386
18. Mundra V, Peng Y, Rana S, Natarajan A, Mahato RI. Micellar formulation of indocyanine green for phototherapy of melanoma. *J Control Release.* 2015;220:130–140. doi:10.1016/j.jconrel.2015.10.029
19. Hsieh C. Phase I clinical trial of curcumin, a chemopreventive agent, in patients with high-risk or pre-malignant lesions. *Anticancer Res.* 2001;21(2895):e2900.
20. Kim TH, Jiang HH, Youn YS, et al. Preparation and characterization of water-soluble albumin-bound curcumin nanoparticles with improved antitumor activity. *Int J Pharm.* 2011;403(12):285–291. doi:10.1016/j.ijpharm.2010.10.041
21. Kim B, Seo B, Park S, et al. Albumin nanoparticles with synergistic antitumor efficacy against metastatic lung cancers. *Colloids Surf B Biointerfaces.* 2017;158:157–166. doi:10.1016/j.colsurfb.2017.06.039
22. Sidhar H, Giri RK. Induction of Bax genes by curcumin is associated with apoptosis and activation of p53 in N2a neuroblastoma cells. *Sci Rep.* 2017;7:41420. doi:10.1038/srep41420
23. Aggarwal B, Singh S, Aggarwal B. Activation of transcription factor NF-kappaB is suppressed by curcumin (diferuloylmethane). *J Biol Chem.* 1995;270:24995–25000. doi:10.1074/jbc.270.42.24995
24. Abe Y, Hashimoto S, Horie T. Curcumin inhibition of inflammatory cytokine production by human peripheral blood monocytes and alveolar macrophages. *Pharmacol Res.* 1999;39(1):41–47. doi:10.1006/phrs.1998.0404
25. Tønnesen HH, Måsson M, Loftsson T. Studies of curcumin and curcuminoids. XXVII. Cyclodextrin complexation: solubility, chemical and photochemical stability. *Int J Pharm.* 2002;244(12):127–135. doi:10.1016/s0378-5173(02)00323-x
26. Anand P, Kunnumakkara AB, Newman RA, Aggarwal BB. Bioavailability of curcumin: problems and promises. *Mol Pharm.* 2007;4(6):807–818. doi:10.1021/mp700113r
27. Kratz F. Albumin as a drug carrier: design of prodrugs, drug conjugates and nanoparticles. *J Control Release.* 2008;132(3):171–183. doi:10.1016/j.jconrel.2008.05.010
28. Thao LQ, Byeon HJ, Lee C, et al. Doxorubicin-bound albumin nanoparticles containing a TRAIL protein for targeted treatment of colon cancer. *Pharm Res.* 2016;33(3):615–626. doi:10.1007/s11095-015-1814-z
29. Ogawara K-I, Furumoto K, Nagayama S, et al. Pre-coating with serum albumin reduces receptor-mediated hepatic disposition of polystyrene nanosphere: implications for rational design of nanoparticles. *J Control Release.* 2004;100(3):451–455. doi:10.1016/j.jconrel.2004.07.028
30. Peng Q, Zhang S, Yang Q, et al. Preformed albumin corona, a protective coating for nanoparticles based drug delivery system. *Biomaterials.* 2013;34(33):8521–8530. doi:10.1016/j.biomaterials.2013.07.102
31. Maeda H, Wu J, Sawa T, Matsumura Y, Hori K. Tumor vascular permeability and the EPR effect in macromolecular therapeutics: a review. *J Control Release.* 2000;65(12):271–284. doi:10.1016/S0168-3659(99)00248-5
32. Sage H, Johnson C, Bornstein P. Characterization of a novel serum albumin-binding glycoprotein secreted by endothelial cells in culture. *J Biol Chem.* 1984;259(6):3993–4007.
33. Tiruppathi C, Song W, Bergenfeldt M, Sass P, Malik AB. Gp60 activation mediates albumin transcytosis in endothelial cells by tyrosine kinase-dependent pathway. *J Biol Chem.* 1997;272(41):25968–25975. doi:10.1074/jbc.272.41.25968
34. Hawkins MJ, Soon-Shiong P, Desai N. Protein nanoparticles as drug carriers in clinical medicine. *Adv Drug Deliv Rev.* 2008;60(8):876–885. doi:10.1016/j.addr.2007.08.044
35. Lee ES, Youn YS. Albumin-based potential drugs: focus on half-life extension and nanoparticle preparation. *J Pharm Invest.* 2016;46(4):305–315. doi:10.1007/s40005-016-0250-3
36. Lin T, Zhao P, Jiang Y, et al. Blood-brain-barrier-penetrating albumin nanoparticles for biomimetic drug delivery via albumin-binding protein pathways for anti-glioma therapy. *ACS Nano.* 2016;10(11):9999–10012. doi:10.1021/acsnano.6b04268
37. Byeon HJ, Lee S, Min SY, et al. Doxorubicin-loaded nanoparticles consisted of cationic-and mannose-modified-albumins for dual-targeting in brain tumors. *J Control Release.* 2016;225:301–313. doi:10.1016/j.jconrel.2016.01.046
38. Thao LQ, Lee C, Kim B, et al. Doxorubicin and paclitaxel co-bound lactosylated albumin nanoparticles having targetability to hepatocellular carcinoma. *Colloids Surf B Biointerfaces.* 2017;152:183–191. doi:10.1016/j.colsurfb.2017.01.017
39. Phuong PTT, Lee S, Lee C, et al. Beta-carotene-bound albumin nanoparticles modified with chlorin e6 for breast tumor ablation based on photodynamic therapy. *Colloids Surf B Biointerfaces.* 2018;171:123–133. doi:10.1016/j.colsurfb.2018.07.016
40. Kim B, Lee C, Lee ES, Shin BS, Youn YS. Paclitaxel and curcumin co-bound albumin nanoparticles having antitumor potential to pancreatic cancer. *Asian J Pharm Sci.* 2016;11(6):708–714. doi:10.1016/j.ajps.2016.05.005

41. Rahman S, Telny T, Ravi T, Kuppusamy S. Role of surfactant and pH in dissolution of curcumin. *Indian J Pharm Sci.* 2009;71(2):139–142. doi:10.4103/0250-474X.54280
42. Liu J, Han J, Kang Z, et al. In vivo near-infrared photothermal therapy and computed tomography imaging of cancer cells using novel tungsten-based theranostic probe. *Nanoscale.* 2014;6(11):5770–5776. doi:10.1039/c3nr06292a
43. Curcio A, Silva AK, Cabana S, et al. Iron oxide nanoflowers@ CuS hybrids for cancer tri-therapy: interplay of photothermal therapy, magnetic hyperthermia and photodynamic therapy. *Theranostics.* 2019;9(5):1288–1302. doi:10.7150/thno.30238
44. Takagi A, Watanabe M, Ishii Y, et al. Three-dimensional cellular spheroid formation provides human prostate tumor cells with tissue-like features. *Anticancer Res.* 2007;27(1A):45–53.
45. Wust P, Hildebrandt B, Sreenivasa G, et al. Hyperthermia in combined treatment of cancer. *Lancet Oncol.* 2002;3(8):487–497. doi:10.1016/s1470-2045(02)00818-5
46. Landon CD, Park JY, Needham D, Dewhirst MW. Nanoscale drug delivery and hyperthermia: the materials design and preclinical and clinical testing of low temperature-sensitive liposomes used in combination with mild hyperthermia in the treatment of local cancer. *Open Nanomed J.* 2011;3:38–64. doi:10.2174/1875933501103010038
47. Lee C, Lim K, Kim SS, et al. Chlorella-gold nanorods hydrogels generating photosynthesis-derived oxygen and mild heat for the treatment of hypoxic breast cancer. *J Control Release.* 2019;294:77–90. doi:10.1016/j.jconrel.2018.12.011
48. Jaque D, Maestro LM, Del Rosal B, et al. Nanoparticles for photothermal therapies. *Nanoscale.* 2014;6(16):9494–9530. doi:10.1039/c4nr00708e
49. Shimizu S, Kamiike W, Hatanaka N, et al. New method for measuring ICG Rmax with a clearance meter. *World J Surg.* 1995;19(1):113–118. doi:10.1007/BF00316992
50. Hill TK, Abdulahad A, Kelkar SS, et al. Indocyanine green-loaded nanoparticles for image-guided tumor surgery. *Bioconjug Chem.* 2015;26(2):294–303. doi:10.1021/bc5005679
51. Saxena V, Sadoqi M, Shao J. Polymeric nanoparticulate delivery system for Indocyanine green: biodistribution in healthy mice. *Int J Pharm.* 2006;308(12):200–204. doi:10.1016/j.ijpharm.2005.11.003
52. Zheng C, Zheng M, Gong P, et al. Indocyanine green-loaded biodegradable tumor targeting nanoprobe for in vitro and in vivo imaging. *Biomaterials.* 2012;33(22):5603–5609. doi:10.1016/j.biomaterials.2012.04.044
53. Wang H, Li X, Tse BWC, et al. Indocyanine green-incorporating nanoparticles for cancer theranostics. *Theranostics.* 2018;8(5):1227–1242. doi:10.7150/thno.22872
54. Sahu A, Lee JH, Lee HG, Jeong YY, Tae G. Prussian blue/serum albumin/indocyanine green as a multifunctional nanotheranostic agent for bimodal imaging guided laser mediated combinatorial phototherapy. *J Control Release.* 2016;236:90–99. doi:10.1016/j.jconrel.2017.09.005
55. Tai X, Wang Y, Zhang L, et al. Cabazitaxel and indocyanine green co-delivery tumor-targeting nanoparticle for improved antitumor efficacy and minimized drug toxicity. *J Drug Target.* 2017;25(2):179–187. doi:10.1080/1061186X.2016.1233975
56. Youn YS, Bae YH. Perspectives on the past, present, and future of cancer nanomedicine. *Adv Drug Deliv Rev.* 2018;130:3–11. doi:10.1016/j.addr.2018.05.008
57. Paulet E, Aubé C, Pessaux P, et al. Factors limiting complete tumor ablation by radiofrequency ablation. *Cardiovasc Intervent Radiol.* 2008;31(1):107–115. doi:10.1007/s00270-007-9208-1
58. Ahmed M, Brace CL, Lee FT Jr, Goldberg SN. Principles of and advances in percutaneous ablation. *Radiology.* 2011;258(2):351–369. doi:10.1148/radiol.10081634
59. Chu KF, Dupuy DE. Thermal ablation of tumours: biological mechanisms and advances in therapy. *Nat Rev Cancer.* 2014;14(3):199–208. doi:10.1038/nrc3672
60. Ceña V, Játiva P. Nanoparticle crossing of blood–brain barrier: A road to new therapeutic approaches to central nervous system diseases. *Nanomedicine.* 2018;13(13):1513–1516. doi:10.2217/nmm-2018-0139
61. Betzer O, Shilo M, Opochnsky R, et al. The effect of nanoparticle size on the ability to cross the blood–brain barrier: an in vivo study. *Nanomedicine.* 2017;12(13):1533–1546. doi:10.2217/nmm-2017-0022
62. De Jong WH, Hagens WI, Krystek P, Burger MC, Sips AJ, Geertsma RE. Particle size-dependent organ distribution of gold nanoparticles after intravenous administration. *Biomaterials.* 2008;29(12):1912–1919. doi:10.1016/j.biomaterials.2007.12.037
63. Narayanan V, Weekes CD. Nanoparticle albumin-bound (nab)-paclitaxel for the treatment of pancreas ductal adenocarcinoma. *Gastrointest Cancer.* 2015;5:11–19. doi:10.2147/GICTT.S55158
64. Yardley DA. nab-Paclitaxel mechanisms of action and delivery. *J Control Release.* 2013;170(3):365–372. doi:10.1016/j.jconrel.2013.05.041
65. Chen N, Brachmann C, Liu X, et al. Albumin-bound nanoparticle (nab): paclitaxel exhibits enhanced paclitaxel tissue distribution and tumor penetration. *Cancer Chemother Pharmacol.* 2015;76(4):699–712. doi:10.1007/s00280-015-2833-5
66. Nichols JW, Bae YH. EPR: evidence and fallacy. *J Control Release.* 2014;190:451–464. doi:10.1016/j.jconrel.2014.03.057
67. Otagiri M, Chuang VTG. *Nanoparticle Albumin-Bound Paclitaxel (Abraxane®) in Albumin in Medicine: Pathological and Clinical Applications.* Springer; 2016:p101–119.

## International Journal of Nanomedicine

### Publish your work in this journal

The International Journal of Nanomedicine is an international, peer-reviewed journal focusing on the application of nanotechnology in diagnostics, therapeutics, and drug delivery systems throughout the biomedical field. This journal is indexed on PubMed Central, MedLine, CAS, SciSearch®, Current Contents®/Clinical Medicine,

Journal Citation Reports/Science Edition, EMBase, Scopus and the Elsevier Bibliographic databases. The manuscript management system is completely online and includes a very quick and fair peer-review system, which is all easy to use. Visit <http://www.dovepress.com/testimonials.php> to read real quotes from published authors.

Submit your manuscript here: <https://www.dovepress.com/international-journal-of-nanomedicine-journal>